



Analysis of the surface deformation characteristics and strata movement mechanism in the main shaft area of Chengchao Iron Mine

Xugen Song^{1,2} · Congxin Chen^{1,2} · Kaizong Xia^{1,2} · Kuoyu Yang^{1,2} · Shan Chen^{1,2} · Xiumin Liu^{1,2}

Received: 5 January 2018 / Accepted: 23 April 2018 / Published online: 4 May 2018
© Springer-Verlag GmbH Germany, part of Springer Nature 2018

Abstract

The surface deformation and strata movement caused by underground mining in a metal mine often exceeds the designed range, which can destroy main shafts and other key structures, causing huge economic losses and affecting production safety. Here, the main shaft area of Chengchao Iron Mine affected by tectonic stress is analyzed. Detailed monitoring data from the past 11 years were used to analyze the surface deformation characteristics and the strata movement mechanism. The results show that the surface deformation in the main shaft area shows S-shaped curve characteristics comprising a stable deformation stage, a rapid deformation stage and a stable deformation stage. The surface horizontal displacement vector in the main shaft area points to the western mining area, indicating that the surface deformation in the main shaft area is mainly affected by underground mining in the western area. From December 2007 to December 2009, the expansion of the movement line ($\epsilon = 2$ mm/m) was small; in December 2009, the expansion of the movement line increased significantly. The expansion law of the break line ($\epsilon = 6$ mm/m) was similar to that of the movement line. Furthermore, the movement angle decreased significantly from December 2009 to December 2011, and the break angle sharply decreased from December 2010 to December 2012. The cantilever beam mechanics model revealed that the fractured width of footwall in the direction of the main shaft area was 266 m. When exploitation reaches a horizontal depth of -600 m, the fracture width is predicted to reach 402 m.

Keywords Metal mine · Underground mining · Main shaft · Field monitoring · Surface deformation · Strata movement mechanism

Introduction

Ground deformation and strata movement induced by underground mining are influenced by many factors, such as the existence of ore bodies, in situ stress, geological structures, hydrogeological conditions, and the mining method (Brady and Brown 1985; Kalenchuk et al. 2008; Wu et al. 2009; Villegas et al. 2011; Villegas Barba and Nordlund 2013; Can et al. 2012; Zhao et al. 2012b, 2013; Li et al. 2013). Thus, when ground deformation exceeds the forecasted deformation, the shaft and related facilities around the mining area will be damaged. This process is common in mines around

the world. For example, in the Tower Colliery mine in New South Wales, Australia, the extent of the mining-impacted area reaches over 1500 m from the mined-out area at a mining depth of only 450 m (Reid 1998; Hebblewhite 2001). The excavation of Xiaoguanzhuang Iron Mine in Shandong, China caused the major deformation of the main and auxiliary shafts which are located approximately 600 m from the mined-out boundary; this seriously affected the normal use of the main and auxiliary shafts (Li et al. 2006, 2009). In the No. 14 ventilating shaft of the Jinchuan No. 2 Mine area, China, underground mining caused a large degree of rock movement and triggered a sudden fall accident, resulting in the filling of a ventilating shaft (Zhao et al. 2012a). In the eastern area of Chengchao Iron Mine, China, the movement angle and break angle of the footwall were both smaller than their designed values, resulting in the deformation and damage of the eastern main shaft and other key buildings (Song et al. 2017).

The main shaft behaves like a throat to transport ore upward in underground mining areas. The stability of a shaft

✉ Kaizong Xia
xiakaizong1988@sina.com

¹ State Key Laboratory of Geomechanics and Geotechnical Engineering, Institute of Rock and Soil Mechanics, Chinese Academy of Sciences, Wuhan 430071, China

² University of Chinese Academy of Science, Beijing 100049, China

can be influenced by many factors (Novikov 1979; Rejeb and Bruel 2001; Bruneau et al. 2003a, b; Yao et al. 2003). Many scholars around the world have addressed the problems of surface deformation and shaft damage caused by underground mining. Bruneau et al. (2003a, b) studied the influence of faults on the stability of the main shaft in the Monte Eesa mine in Australia using comprehensive numerical modeling and theoretical analysis method and found that there was a compression zone resulting in vertical displacement around the shaft. Li et al. (2009) analyzed the reasons for the deformation of the main and auxiliary shafts located outside the traditional “movement angle” in Xiaoguanzhuang Iron Mine and found that the shaft damage is affected by regional horizontal displacement. Ma et al. (2013) and Zhao et al. (2012a) analyzed the damage mechanism of the ventilating shaft based on a comprehensive consideration of geological conditions, underground excavations, and numerical simulations and found that the steep dip angle of the ore body and fault/fissures was responsible for the shaft damage.

Although the abovementioned studies have revealed some of the causes of shaft deformation and damage, most of these studies are based on theoretical analysis and numerical calculations, and they lack reliable monitoring data. In this study, based on the monitoring data of surface and deep rock mass deformation obtained over the past 11 years, combined with the analysis of the mechanism of strata movement, the ground deformation characteristics and strata movement mechanism are analyzed in the main shaft area of Chengchao Iron Mine, China.

Description of the mine

Engineering geology and mining situations

Chengchao Iron Mine is located in Ezhou City, Hubei Province, China. It is the third largest iron mine in China (after Meishan Iron Mine and Jingtieshan Iron Mine), with an annual output of over 3 million tons of ore. The ore body is approximately 3000 m long (E–W) and 1500 m wide (N–S). The topography of the ore district comprises hilly landforms, and the ridge extends to the NWW. The rock mass surrounding the footwall is granite, and the hanging wall near the ore body is diorite. Four main groups of joints in the footwall in the west area are found through field investigation, which strike NNW, NWW, NE, and NEE. The NNW-striking joints are the most developed, with a joint density of 3–10/m and an occurrence of $74 \angle 82^\circ$ (Song and Chen 2013; Chen et al. 2017).

Metal mines may subject to frequent intensive tectonic movements in the formation of their ore bodies. In such mines, their horizontal tectonic stress fields are greater than their vertical stress fields (Cai et al. 2000;

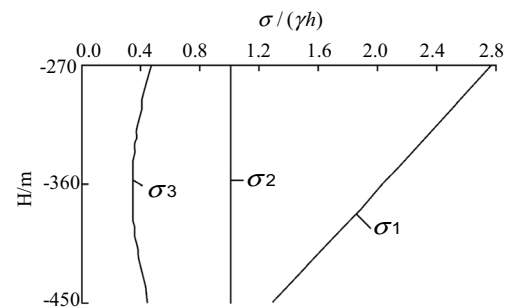


Fig. 1 Diagram of principal stress distribution in Chengchao iron mine

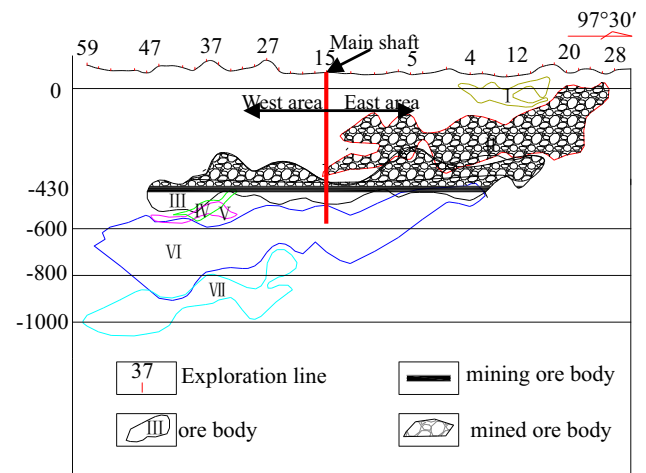


Fig. 2 Projection of main ore body

Hebblewhite 2001; Li et al. 2004; Zhao et al. 2012b, 2013; Tan et al. 2014). As reported by Xia et al. (2016), a large horizontal tectonic stress field exists in the surrounding rock mass in the Chengchao Iron Mine. The direction of maximum principal stress (σ_1) is $N75^\circ W-N85^\circ W$, which is consistent with the strike of the ore body, and the maximum principal stress of Chengchao Iron Mine is very high, approaching $2.8\gamma h$ (19.5 MPa) at -270 m (Fig. 1). The direction of minimum principal stress (σ_3) is approximately perpendicular to the strike of the ore body. The intermediate principal stress (σ_2) corresponds to the self-weight stress of the rock mass.

Chengchao Iron Mine is divided into eastern and western areas by the #15 exploration line. The I, II, and III ore bodies are located in the eastern mining area, and the III, IV, V, VI, and VII ore bodies are located in the western mining area (Fig. 2). The eastern mining area was mined from the -16 m level in 1970, and the western mining area was mined from the -290 m level in 2002. The mining method is sublevel caving without sill pillars. Descriptions of the mining situations in the western and eastern areas are listed

Table 1 Mining situations in western mining area

Mining level (m)	Mining date		Mining ore body
	Beginning	End	
–290.0	2002–07	2004–07	#III
–307.5	2002–11	2004–07	#III
–325.0	2003–05	2004–12	#III
–342.5	2004–07	2006–12	#III
–358.0	2005–10	2008–09	#III
–375.5	2007–07	2012–06	#III
–393.0	2009–05	2015–01	#III
–410.5	2012–03	2017–01	#III
–430.0	2014–07		#III
–447.5	2017–05		#III

Table 2 Mining situations in eastern mining area

Mining level (m)	Mining date		Mining ore body
	Beginning	End	
–16.0	1970–01	1978–01	#I and #II
–106.0	1979–01	1984–01	#II
–160.0	1984–01	1990–01	#II
–218.0	1990–01	1997–01	#II
–260.0	1998–01	2002–01	#II
302.0	2002–01	2007–07	#II
–375.5	2007–07	2012–06	#III
–393.0	2009–05	2013–12	#III
–410.5	2013–03	2017–01	#III
–430.0	2014–07		#III
–447.5	2016–06		#III

in Tables 1 and 2. Currently, the –430 and –447.5 m levels are being mined.

Description of the main shaft area

The main shaft of Chengchao Iron Mine is located in the #15 exploration line of the footwall (Fig. 2), which is the dividing line between the eastern and western areas of Chengchao Iron Mine. Operation of the main shaft began in 1989 with a total investment of ¥36.99 million (CNY) (currently equivalent to approximately ¥370 million or 56 million dollars). The depth of the main shaft is 635 m, the bottom elevation is –550 m, and the tower height is 71.2 m (Fig. 3). The transportation capacity of the main shaft is to upgrade 1.5 million tons of ore and 275,000 tons of waste rock each year. This project won second place in the Sixth Excellent Engineering Design competition of the Chinese Ministry of Metallurgy in 1992. After its completion, it became the most important main shaft in Chengchao Iron Mine. The main facilities of

the main shaft area include not only the main shaft, but also the western ventilating shaft, railway, mine road, and transportation tunnel (Fig. 4).

Due to the effects of underground mining, the ground of the main shaft area, the wall, and the machine room became cracked in 2012 (Fig. 5a–c), and the main shaft had to stop being used in 2015. The total service life of the main shaft was only 26 years; the loss of the main shaft before its designed time caused huge losses to Chengchao Iron Mine.

Investigation of ground deformation

Monitoring method and implementation process

Underground mining will lead to the deformation of the surface and the deep rock mass first, resulting in the destruction of the building and facilities. To assess the surface deformation induced by underground mining, the global positioning system (GPS) monitoring technique was applied to the mining-influenced area in 2006 after the collapse pits occurred in western mining area, and the monitoring network was established using Topcon Hiper-II GPS receivers with accuracy in the horizontal direction to 5 and 20 mm in the vertical direction. To improve the monitoring accuracy, the vertical displacement was monitored by a Leica Automatic Level. A total of 130 GPS monitoring points and 103 level monitoring points were obtained. Among these monitoring points, 13 GPS monitoring points and 21 level points were located in the main shaft area, as shown in Table 3. The locations of these monitoring points are shown in Figs. 10 and 11. After the ground of the main shaft area experienced the rapid deformation stage, cracks were generated in the walls and the machine room. The expansion of the cracks was monitored. The locations of the monitoring points are shown in Fig. 3; numbers S4–S7 are wall cracks and S4–S7 are machine room cracks. Meanwhile, to assess the deformation of the deep rock mass, the horizontal displacement of the deep rock mass in the main shaft area has been monitored since August 2011. The monitoring instrument utilizes a 50325-M drilling inclinometer from the SINCO Corporation of the United States. The location of the drill hole is shown in Fig. 4.

Monitoring results

By analyzing monitoring data collected over nearly 11 years (from 2006 to 2017), the deformation law of the surface and deep rock masses is revealed in the main shaft area of Chengchao Iron Mine.

1. Based on GPS and level monitoring data, the monitoring results of the typical monitoring points in the main shaft area are listed in Tables 4 and 5, and the horizontal

Fig. 3 Current situations in main shaft area of Chengchao iron mine took by UAV

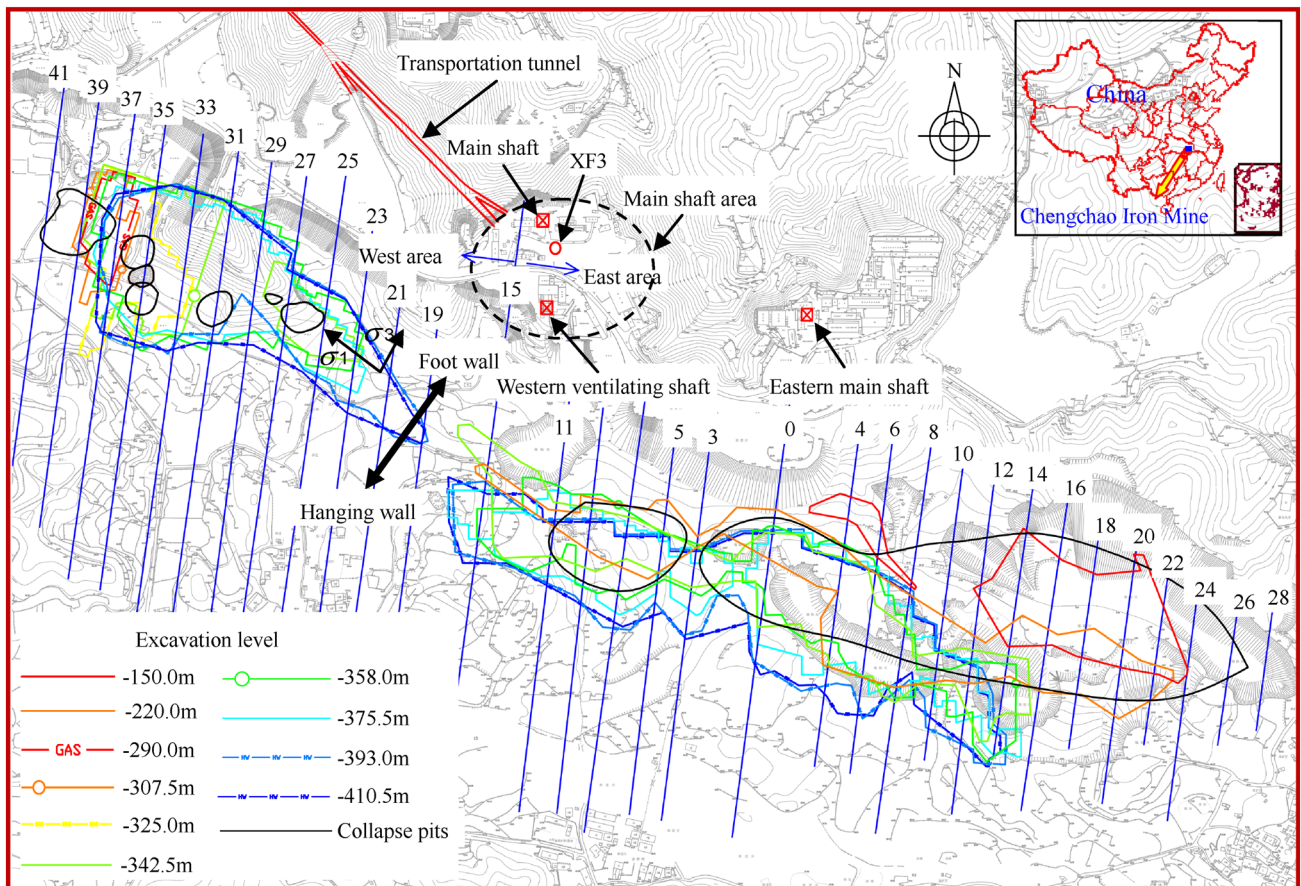
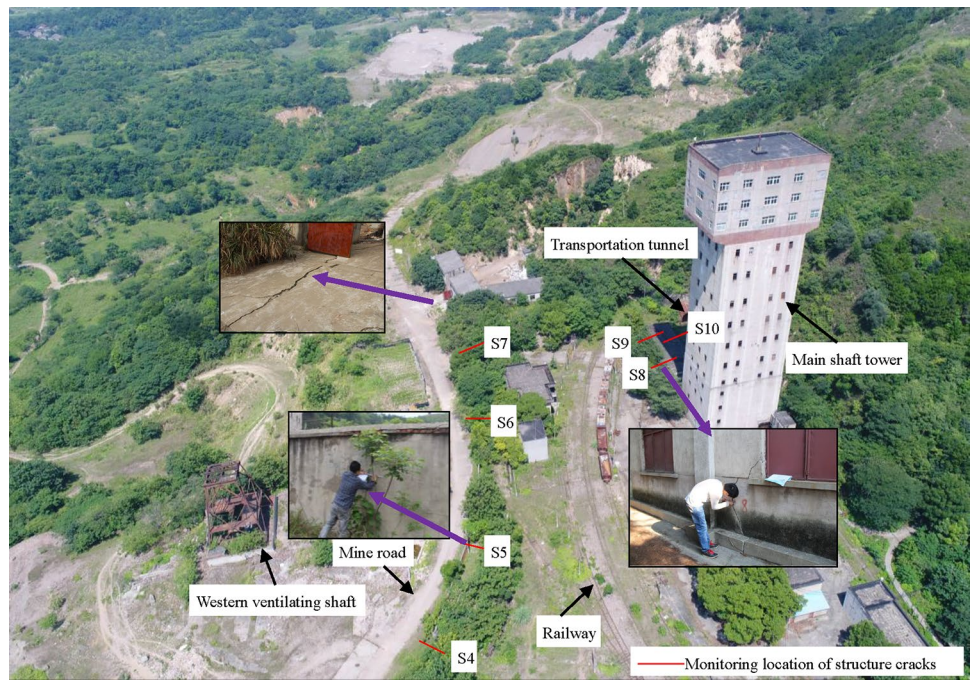


Fig. 4 Horizontal projection of mined-out boundaries and location of the main shaft

Fig. 5 Ground and structure damage in main shaft area



Table 3 Monitoring situations

Monitoring period	The total number of GPS points (located in main shaft area)	The total number of level points (located in main shaft area)	Monitoring frequency
2006–Present	130 (13)	103 (21)	Once a month

Table 4 Ratio of cumulative horizontal-to-vertical displacement from September 2007 to September 2015 (unit: cm)

Monitoring points	DC25	DC24	DS02	DS01
Cumulative horizontal displacement	24.9	30.1	20.4	19.8
Cumulative vertical displacement	-24.0	-16.6	-9.4	-10.9
Ratio of cumulative horizontal displacement to cumulative vertical displacement	1.04	1.81	2.17	1.82

Table 5 Cumulative displacement of representative monitoring points from September 2007 to July 2017 in main shaft area (unit: cm)

Monitoring points	N	E	H	V	Deformation direction	E/N
DC24	-10.0	-40.1	41.4	-20.4	SW	4.0
DC25	-6.1	-36.5	37.0	-29.0	SW	6.0
DS01	-6.0	-19.9	20.7	-4.9	SW	3.3
DS02	-2.6	-23.5	23.6	-9.9	SW	9.0

displacement curves of the monitoring points from August 2007 to July 2017 and the vertical displacement curves from August 2007 to October 2015 in the main shaft area are plotted in Fig. 6. Based on the monitoring results of the cracks in the wall and the machine room, the curves of crack expansion over time are plotted in Fig. 7. The curve of the ratio of the horizontal displacement to the vertical displacement of typical monitoring points is plotted in Fig. 8.

2. The horizontal displacement vector diagram of the main shaft area from June 2006 to July 2017 was drawn with Surfer (Fig. 9); this diagram accurately reflects the direction of ground deformation in the main shaft area.

3. According to the definitions of the movement line (defined as a horizontal strain at the surface of $\epsilon = 2 \text{ mm/m}$) and the break line (defined as a horizontal strain at the surface of $\epsilon = 6 \text{ mm/m}$), the maps of the movement line and break line in the main shaft area from December 2007 to July 2017 are plotted in Figs. 10 and 11, and the histograms of the annual expansion of the movement line and break line are shown in Figs. 12 and 13, respectively. According

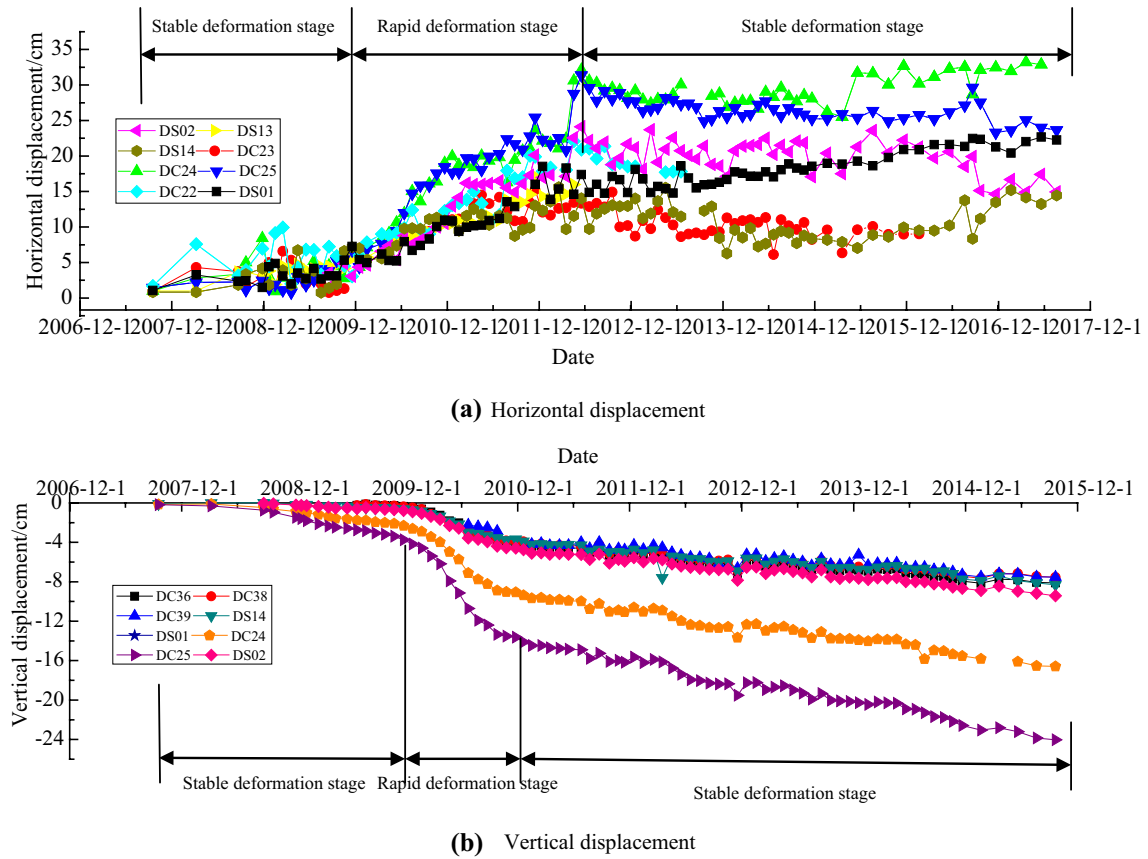


Fig. 6 Cumulative displacement curve over time of monitoring points in the main shaft area

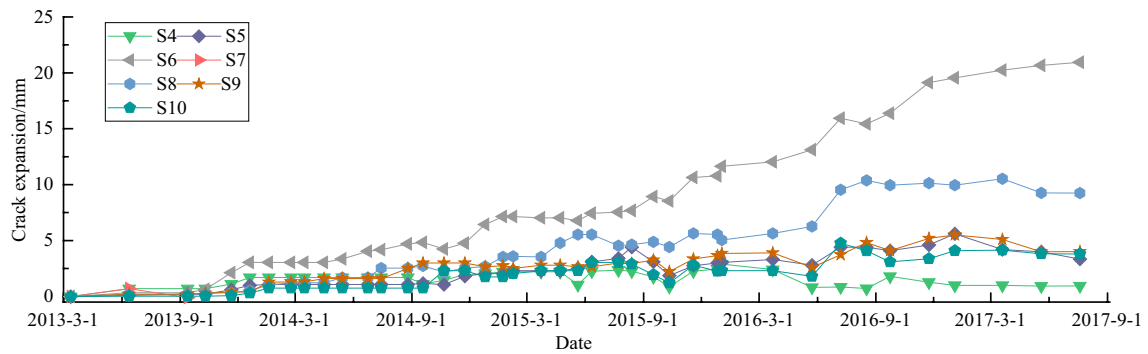


Fig. 7 Curves of the crack propagation of structures in the main shaft area over time

to the definition of the movement angle (defined as the angle between the line connecting the movement line to the boundary of the mined-out area and a horizontal line) and the break angle (defined as the angle between the line connecting the break line to the boundary of the mined-out area and a horizontal line), the extension of the movement angle of the #I profile in the main shaft area from December 2007 to July 2017 and the break angle from December 2010 to July 2017 is plotted in Figs. 14 and 15, respectively.

4. The cumulative horizontal displacement of the deep rock mass from August 2011–July 2017, based on the results of deep rock monitoring, is plotted in Fig. 16.

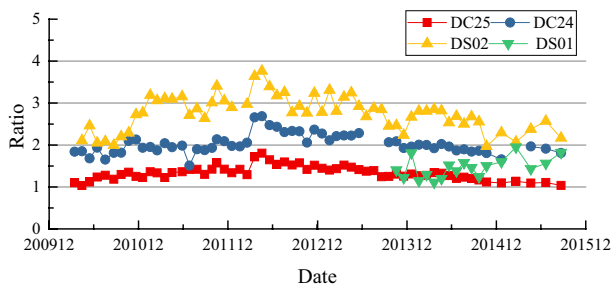


Fig. 8 Curves of ratio of cumulative horizontal-to-vertical displacement over time

Analysis of ground deformation and building damage characteristics in the main shaft area

The cumulative displacement curves of the monitoring points in the main shaft area over time (Fig. 6) are S-shaped curves. The curves first increase in a stable manner, then enter a rapid growth phase, and finally increase in a stable manner again. The rapid deformation stage of vertical displacement lasted from December 2009 to December 2010, and the rapid deformation stage of

horizontal displacement lasted from December 2009 to May 2012. The horizontal displacement continued to rapidly increase for some time after the vertical displacement resumed its stable stage. From August 2007 to December 2009, the deformation of the ground increased steadily, and the monthly deformation was small. For example, the DS02 monitoring point had a total horizontal displacement of 43.5 mm and a cumulative vertical displacement of -9.0 mm in December 2009, with an average monthly horizontal displacement of 1.6 mm and an average monthly vertical displacement of only -0.3 mm. In December 2009, there was a phase of rapid surface deformation. For example, the accumulated horizontal displacement of the DS02 monitoring point reached 241.0 mm in May 2012, and the average monthly horizontal displacement was 6.8 mm from December 2009 to December 2010; this value was 4.3 times larger than the average monthly horizontal displacement from August 2007 to December 2009. The cumulative vertical displacement in December 2010 was -47.5 mm and the average monthly vertical displacement from December 2009 to December 2010 was -3.2 mm, which was 10.7 times larger than the average monthly vertical displacement from August 2007 to December 2009. After the rapid deformation stage, the deformation returned to a stable deformation stage,

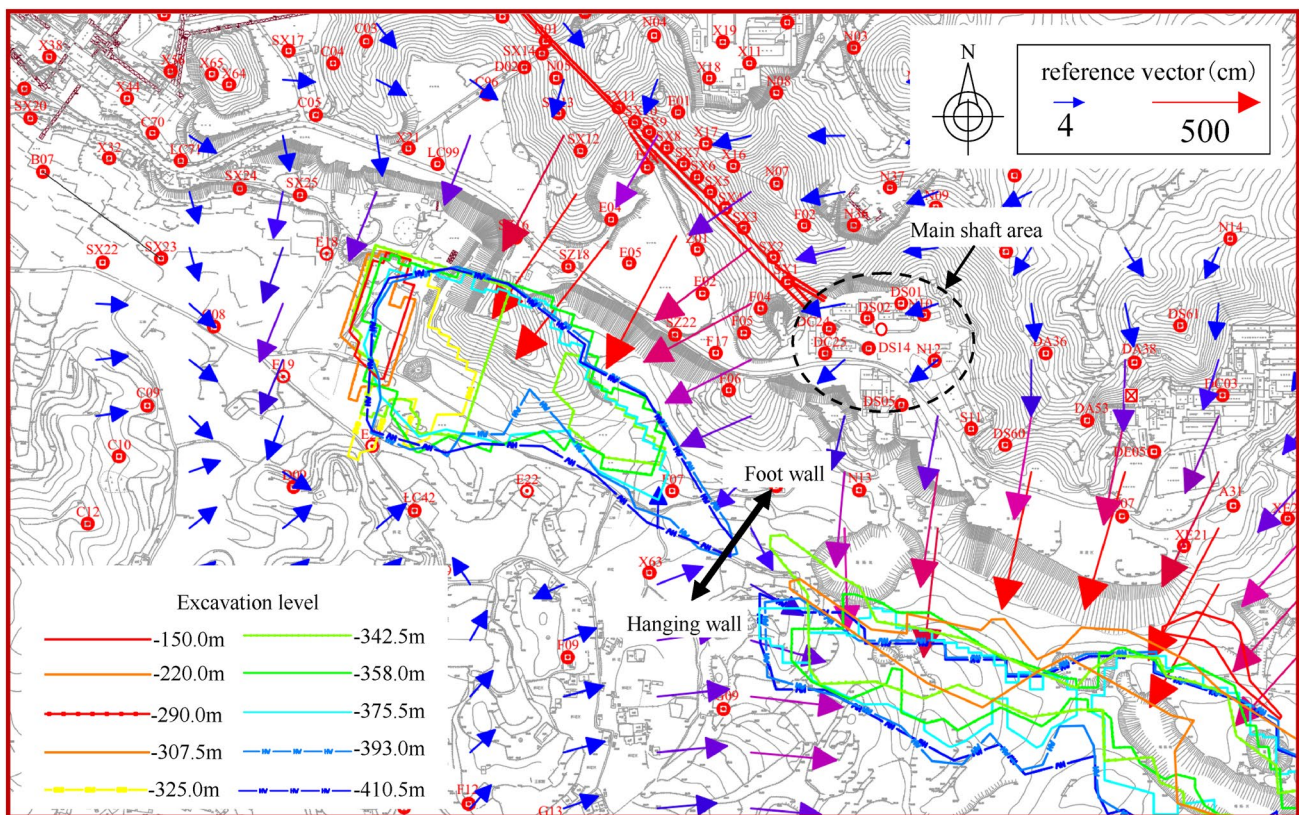


Fig. 9 Horizontal displacement vector diagram from June 2006 to July 2017 of the main shaft area

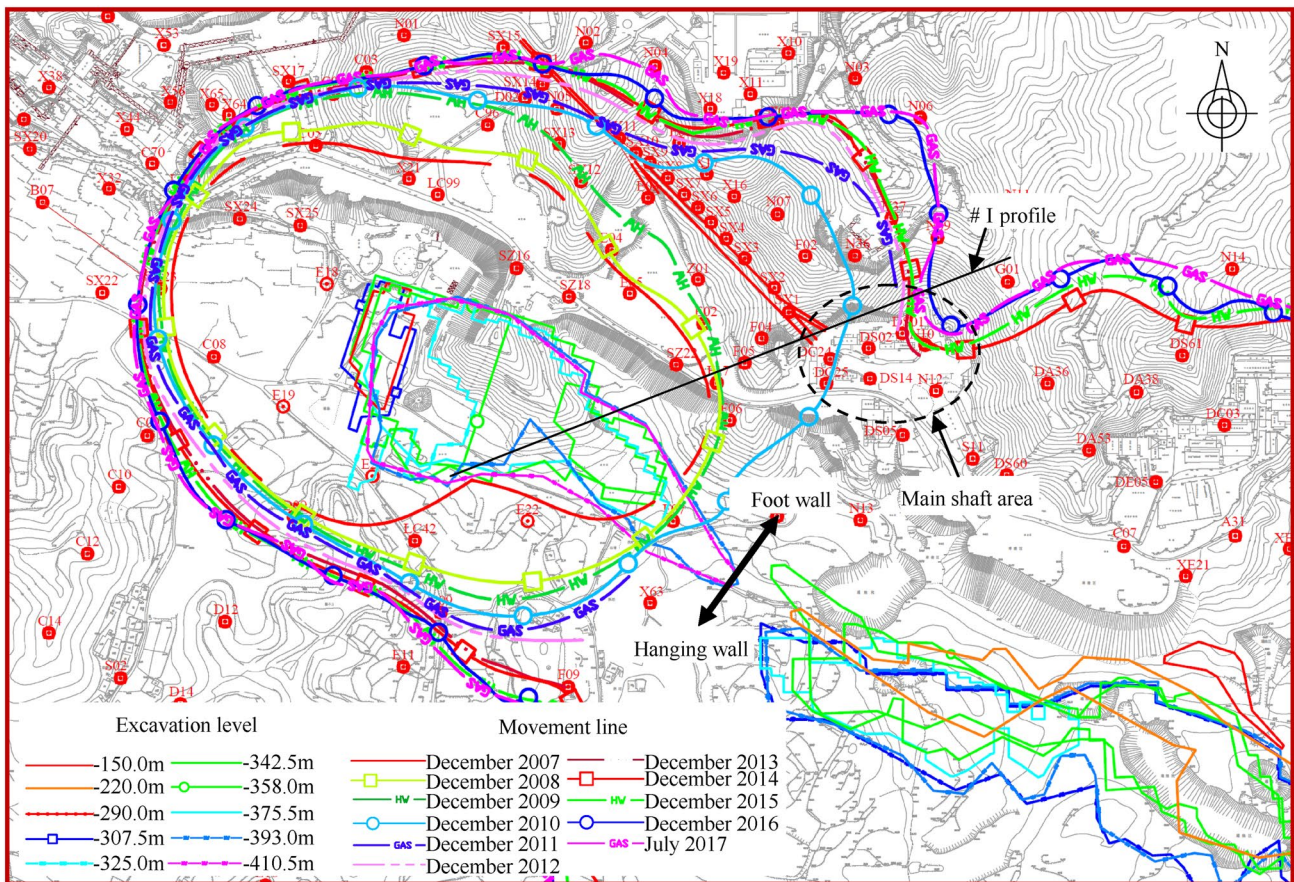


Fig. 10 Map of movement line in the main shaft area from December 2007 to July 2017 (all the red numbers refer to GPS monitoring points)

indicating that in the main shaft area, the deep rock mass was fractured during the rapid deformation stage and the horizontal tectonic stress at the rock mass was released. Due to the influence of tectonic stress, the duration of the horizontal rapid deformation stage lasted until May 2012, which was longer than the vertical rapid deformation stage.

Figure 7 demonstrates that the expansion speed of cracks in key buildings is stable. The width of the fastest expanding crack, S6, expanded by 20.94 mm from March 2013 to July 2017, with an average expansion of 0.57 mm per month. The slowest expanding crack is S4, which had an accumulated expansion width of 0.94 mm and an average monthly expansion width of only 0.02 mm. Figure 6 shows that the surface deformation was stable from March 2013 to July 2017, corresponding to the stable expansion of cracks, indicating that there is consistency between surface deformation and the expansion of cracks in the main shaft area.

Table 4 shows that the cumulative horizontal displacement in the main shaft area is greater than the vertical displacement. The ratio of the cumulative horizontal displacement to the vertical displacement of DC25, which is

closest to the western mined-out area, is 1.04. The ratio of the cumulative horizontal displacement to the vertical displacement of DC24, which is slightly farther from the western mined-out area, is 1.81. In addition, the ratios at DS02 and DS01 are 2.17 and 1.82, respectively. Figure 8 shows that over time, the ratio of horizontal displacement to vertical displacement first increases and then decreases, reaching its maximum value in May 2012. The reason for this phenomenon is that the vertical deformation stabilized in 2010, whereas the period of horizontal displacement acceleration lasted until May 2012. This timing difference results from the large horizontal tectonic stress in the footwall of Chengchao Iron Mine (Fig. 1).

Figure 9 shows that the horizontal displacement vector of the main shaft area points to the western mining area of Chengchao Iron Mine, indicating that the surface deformation in the main shaft area is mainly affected by the underground mining in the western area. Table 5 shows that the horizontal displacement in the E direction is much larger than that in the N direction. For example, at monitoring point DC24, the deformation of the cumulative horizontal deformation from September 2007 to July 2017 is

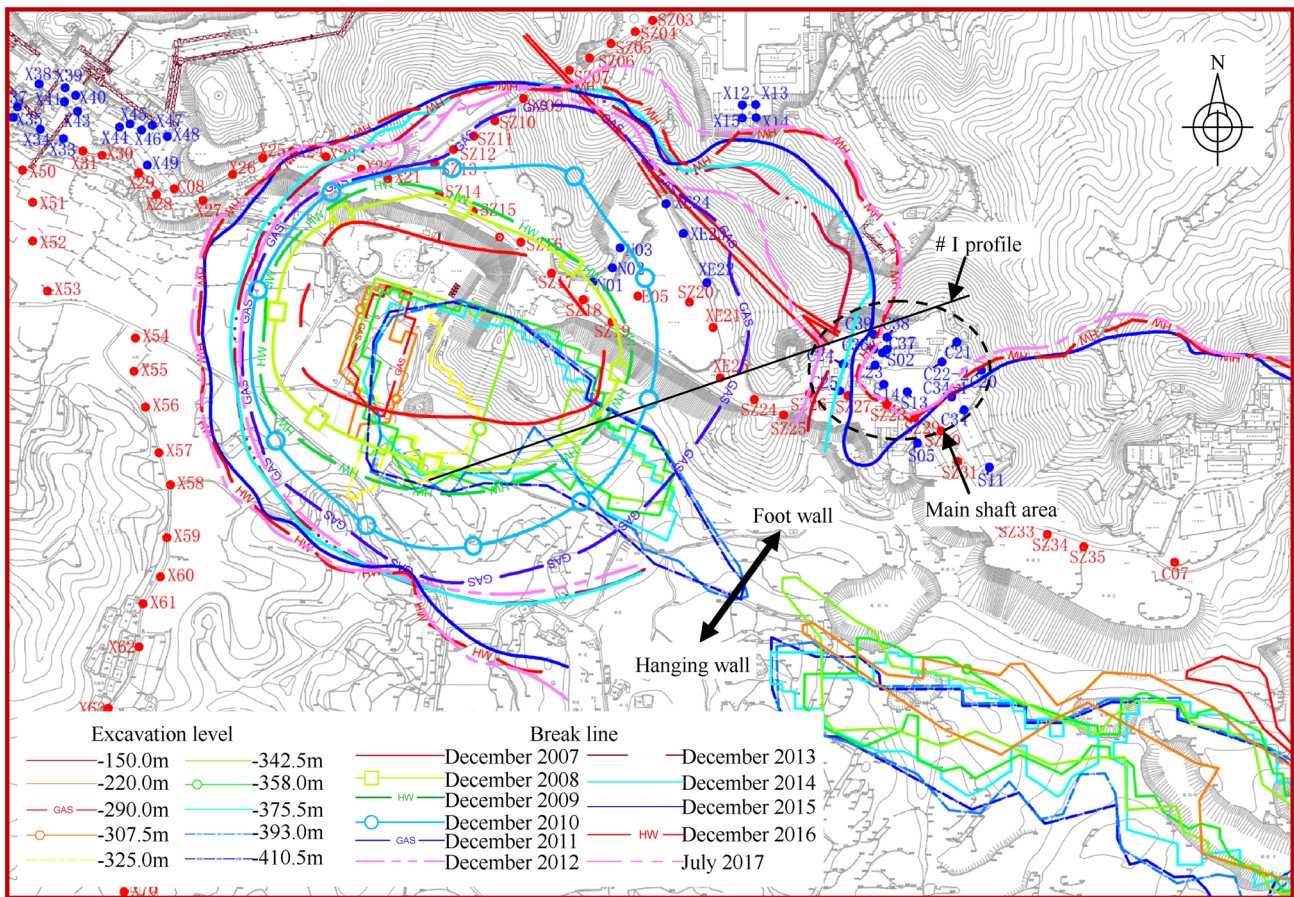


Fig. 11 Map of break line in the main shaft area from December 2007 to July 2017 (all the red and blue numbers refer to level monitoring points)

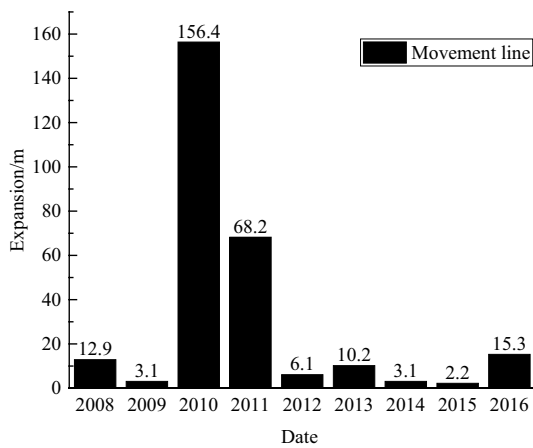


Fig. 12 Histogram of annual expansion of movement line on #I profile

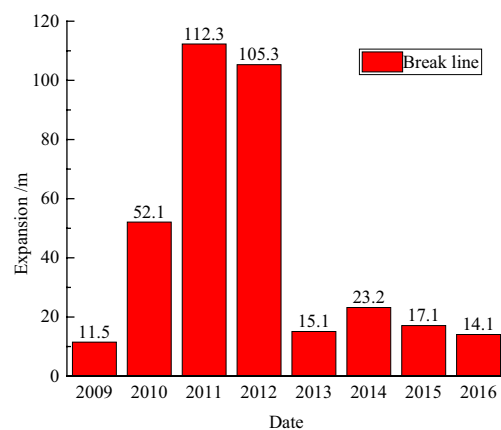


Fig. 13 Histogram of annual expansion of break line on #I profile

– 40.1 cm in the E direction (the negative sign indicates the westward displacement) and the deformation in the N direction is – 10.0 cm (the negative sign indicates the

southward displacement). Hence, the deformation in the E direction is 4.0 times greater than that in the N direction, which demonstrates that the main shaft area is less

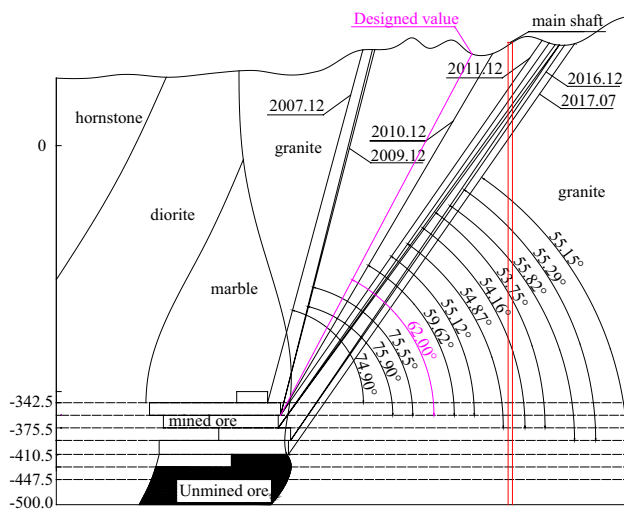


Fig. 14 Movement angle of #I profile

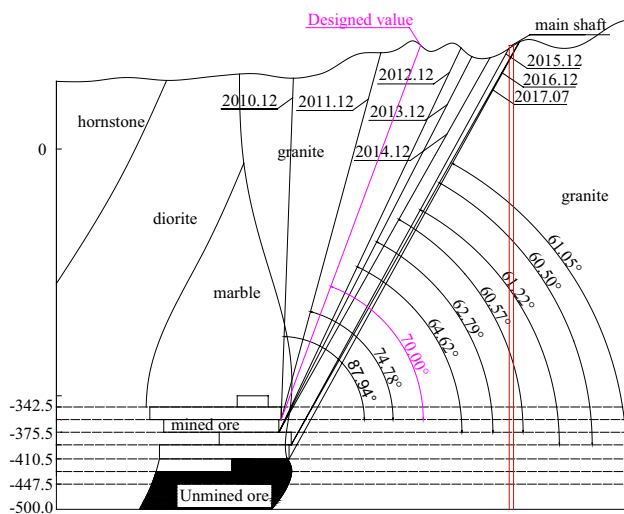


Fig. 15 Break angle of #I profile

affected by the underground mining of the eastern mining area (which is located south of the main shaft).

The expansion of the movement line can be seen in Figs. 10 and 12. The movement line expanded slightly in the direction of the main shaft area from December 2007 to December 2009, with a cumulative expansion distance of only 16.0 m. Since 2009, the movement line of the western area expanded rapidly in the direction of the main shaft area. By December 2010, the movement line had reached the machine room of the main shaft but had not yet reached the tower of the main shaft. From December 2009 to December 2010, the expansion distance was 156.4 m, which is 9.8 times the total expansion distance from December 2007 to December 2009. By December 2011, almost the entire main shaft area had entered the movement area (i.e., the

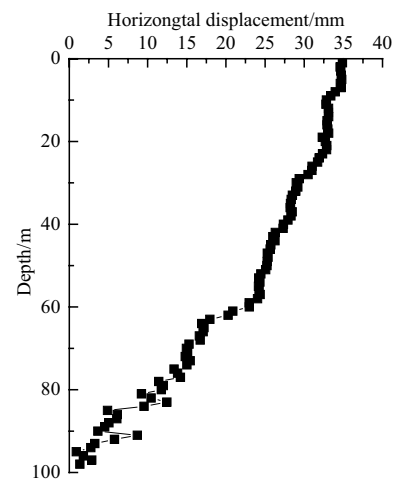


Fig. 16 Curves of the displacement with depth at the drill hole XF3

area within the movement line). The cumulative expansion distance from December 2010 to December 2011 was 68.2 m, and the expansion distance from December 2009 to December 2011 was 14.0 times the expansion distance from December 2007 to December 2009. After December 2011, the expansion of the movement lines resumed its stability. From December 2011 to July 2017, the cumulative expansion distance was only 36.9 m, with an average annual expansion of 7.4 m.

The expansion of the break line can be seen from Figs. 11 and 13. The break line from December 2008 to December 2009 expanded by only approximately 11.5 m. From December 2009 to December 2010, the expansion of the break line was approximately 52.1 m, which is 4.5 times the expansion distance from December 2008 to December 2009. From December 2010 to December 2011, the expansion of the break line was 112.3 m, which is 9.8 times the expansion distance from December 2008 to December 2009. From December 2011 to December 2012, the monthly expansion distance was 110.2 m, which is 9.6 times the total expansion distance from December 2008 to December 2009. After December 2011, the expansion of the break line returned to a stable level but continued expanding. By December 2015, the machine room entered the break area (the area within the break line). In December 2016, the shaft entered the break area. From December 2012 to July 2017, the expansion distance of the break line was 69.5 m, with an average expansion of 17.4 m per year.

From 2012 to 2015, the maintenance costs of the buildings in the main shaft area (including the transportation tunnel, the machine room, the mine road and wall) amounted to more than ¥30 million (CNY) (equivalent to approximately 4.5 million dollars) (Chen et al. 2016). Figure 10 shows that the main shaft area entered the movement area in December 2011. When the main shaft area enters the movement area,

the normal use of buildings will be affected, but they can continue to be used after maintenance. In December 2015, the machine room of the main shaft entered the break area, and the minimum distance between the shaft tower and the break line was only 5.8 m, indicating that buildings could not continue to be used after entering the break area.

Strata movement mechanism

Deformation and movement characteristics of the rock mass in the main shaft area

1. Figure 14 shows that from December 2007 to December 2009, the movement angle basically remained unchanged. From December 2009 to December 2010, the movement angle sharply decreased from 75.90° to 59.62° , representing a decrease of 16.28° . From December 2010 to December 2011, the movement angle decreased by 4.50° to 55.12° . This value is less than the designed value of 62° (Song and Chen 2013). From Fig. 14, we can see that main shaft is outside the designed range of the movement angle. When the actual movement angle becomes less than the designed value, buildings and facilities originally arranged outside the movement area enter the movement area, leading to cracks in the main shaft and other facilities. After December 2011, although the movement line continued to expand slowly, the movement angle essentially did not change from December 2011 to July 2017 due to the continuous deepening of the mining.

2. From December 2010 to December 2011, the break angle changed from 87.94° to 74.76° , decreasing by 13.18° . From December 2011 to December 2012, the break angle changed from 74.76° to 64.62° , decreasing by 10.14° . After December 2012, the decrease rate of the break angle slowed. The designed value of the break angle of the footwall in the western mining area was 70° , which is based on the experience of the eastern mining area. In July 2017, the break angle of the footwall in the western area was 61.05° , which is 9.95° smaller than the designed value. As shown in Fig. 15, the main shaft is outside the designed range of the break angle. When the actual break angle becomes less than the designed value, buildings and facilities originally located outside the break area enter the break area, leading to the abandonment of the main shaft and other facilities.

3. The above analyses indicate that the deformation and failure of the main shaft area were closely related to the sharp decreases of the movement and break angles that occurred from December 2009 to December 2012. As shown in Fig. 1, there is a large horizontal tectonic stress in Chengchao Iron Mine, and the NNW-striking joints are very developed in main shaft area. The main reasons causing the movement and break angles to become smaller than the

designed value are the larger horizontal tectonic stresses and the developed joints. Therefore, when planning and designing other similar metal mines in the future, the influence of joints and tectonic stresses should be fully considered. The key structures should not be located in the areas where the joints are developed. If this cannot be avoided, the designed values of the movement and break angles should be reduced correspondingly so that the key buildings can be located outside the movement and break areas.

4. Figure 16 demonstrates that no obvious sliding failure was observed in the deep rock mass in the main shaft area, indicating that the failure mode of the deep rock mass in the main shaft area was not a type of shear slip.

Strata movement mechanism in the main shaft area

Aydan and Kawamoto (1992), Adhikary et al. (1997) and Adhikary and Dyskin (2007) studied the stress conditions and critical failure conditions of cantilever beams of rock mass, and Pinheiro et al. (2015) used the distinct element method to study the flexural toppling failure. Xia et al. (2017) and Cheng et al. (2017) introduced the cantilever beam stress conditions and critical failure conditions into the analysis of the strata movement mechanism of Chengchao Iron Mine. It is considered that the rock mass of the footwall of the western area of Chengchao Iron Mine is cut into cantilever beams by the NNW-striking joints and that toppling failure has occurred (Figs. 17, 18, 19). The main shaft area is located at the junction of the eastern and western areas of Chengchao Iron Mine. Previous analyses have shown that the deformation of the surface and rock mass in the main shaft area is mainly affected by underground mining in the western mining area under the combined effects of joints and horizontal tectonic stress. Therefore, the strata movement mechanism in the main shaft area can be analyzed using the cantilever beam toppling failure theory.

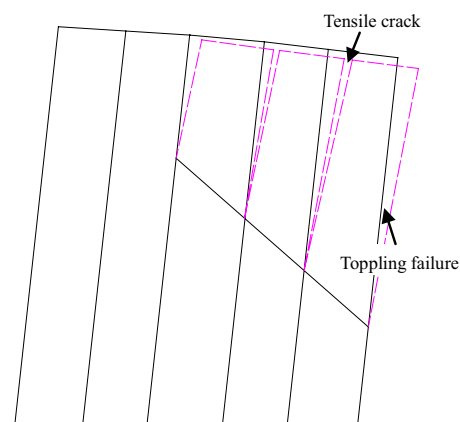


Fig. 17 Schematic diagram of toppling failure

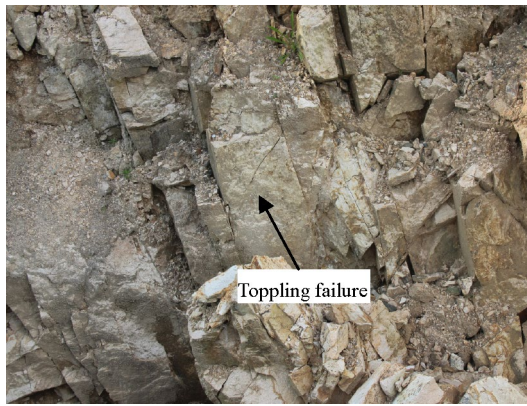


Fig. 18 Toppling failure in the footwall of west area



Fig. 19 Tensile crack around main shaft area

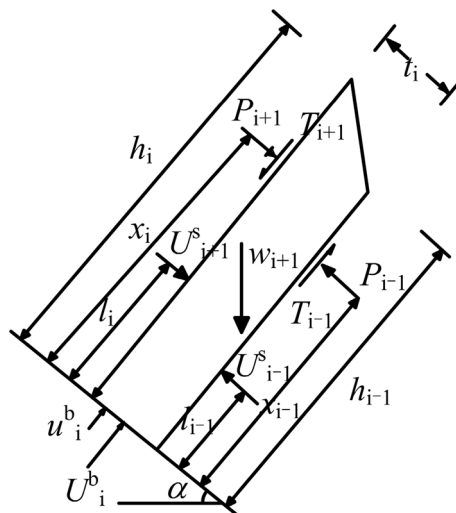


Fig. 20 Free-body diagram of cantilever beam limiting equilibrium model

Based on the free-body diagram of the cantilever beam limit equilibrium model (Fig. 20), Aydan and Kawamoto (1992) derived the following equation:

$$P_{(i-1)} = \frac{P_{(i+1)}\left(\eta h_i - \mu_i \frac{t_i}{2}\right) + R_i \frac{\bar{h}_i}{2} - \frac{2I_i}{t_i}\left(\sigma_t + \frac{N_i}{A_i}\right)}{\left(\eta h_{i-1} + \mu_i \frac{t_i}{2}\right)}, \quad (1)$$

where $W_i = \gamma t_i \bar{h}_i$, $I_i = t_i^3 / 12$, $R_i = W_i \sin \alpha$, $N_i = W_i \cos \alpha$, $\mu_i = \tan \varphi_i$, and $\bar{h}_i = 0.5(h_i + h_{i-1})$; R_i is the component of gravity perpendicular to the cantilever beam, N_i is that in the axial direction, α is the inclination of the cantilever beam, t_i is the thickness of the layer, γ is the weight of the material, φ_i is the frictional angle, and A_i is the area of the bottom surface of the cantilever beam, which is equal to t_i in the per unit length condition.

For the first cantilever beam, $P_{(i+1)} = K\gamma h^2 / 2$. K is the lateral pressure coefficient, and $P_{(i-1)}$ is the lateral pressure near the side of the mined-out area. After surface collapse occurs, $P_{(i-1)} = 0$. Let $\bar{h}_i = h_i = h_{i-1} = h$ (h is the height of the cantilever beam). Equation 1 can then be rewritten as follows:

$$\frac{1}{2}k\gamma\eta h^3 - \frac{1}{4}k\gamma t_i h^2 \tan \varphi_i + \frac{1}{2}\gamma t_i h^2 \sin \alpha - \frac{1}{6}t_i^2 \sigma_t - \frac{1}{6}\gamma t_i^2 \cos \alpha = 0 \quad (2)$$

Based on the previously mentioned tectonic stress test results, the direction of the main shaft is the direction of minimum principal stress, which can be expressed as $\sigma_3 = 0.4\gamma h$; thus, $K = 0.4$. Because the rock mass of the main shaft area is granite, according to the test results of the Institute of Rock and Soil Mechanics, Chinese Academy of Sciences (Chen et al. 2014), $\gamma = 25 \text{ KN/m}^3$ and $\varphi_i = 38.9^\circ$, and the tensile strength of the granite $\sigma_t = 1 \text{ MP}$. The inclination of the cantilever beam is 82° ; thus, $\alpha = 90^\circ - 82^\circ = 8^\circ$. According to Aydan and Kawamoto (1992), $\eta = 1/3$; thus, Eq. 2 can be simplified as follows:

$$1666.7h^3 - 277.5t_i h^2 - 166666.7t_i^2 - 4126.1ht_i^2. \quad (3)$$

This equation can be solved using MATLAB, and the resulting curve is shown in Fig. 21. By December 2009, most of the ore at the level of -375.5 m in the western area of Chengchao Iron Mine had been mined. At the level of -393 m , only a few ore bodies had been mined in the southern part of the western area (as the mining progressed from south to north). With a mining depth of -375.5 m and an elevation of the ground surface in the main shaft area of 85 m , the calculated height of the cantilever beam is 460.5 m . Figure 21 shows that to prevent the cantilever beam from fracturing, the width of the cantilever should be 266 m , but the actual joint density is $3\text{--}10/\text{m}$. Hence, the toppling failure of the cantilever beam can be considered to have occurred within a distance of at least 266 m from the

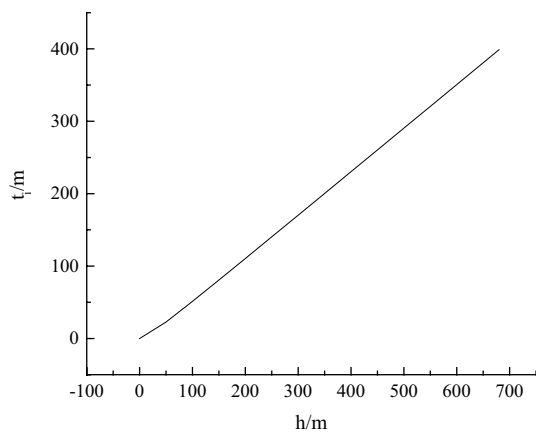


Fig. 21 Relationship between h and t_i

mined-out area. The actual distance from the main shaft area to the western mined-out area is approximately 270 m. This also means that the accelerated deformation of the ground in December 2009 and the sharp decrease of the movement and break angles during 2010–2012 in the main shaft area were due to the fracturing and toppling failure of the deep rock mass, which resulted in the release of tectonic stress.

When the underground mining depth reaches -600 m, the height of the cantilever beam will reach 685 m, and the width of the toppling failure of the cantilever beam will reach 402 m (Fig. 21).

Conclusions

By analyzing monitoring data in the main shaft area, the deformation characteristics and the strata movement mechanism are revealed as follows:

1. The surface deformation curves in the main shaft area were deemed to be S-shaped curves comprising a stable deformation stage, a rapid deformation stage and a stable deformation stage. The rapid deformation stage of horizontal displacement lasted longer than that of vertical displacement due to the tectonic stress conditions of Chengchao Iron Mine.

2. The horizontal displacement vector of the main shaft area points to the western area of Chengchao Iron Mine. The horizontal displacement in the E direction is 3.3–9.0 times that in the N direction, indicating that the surface deformation in the main shaft area is mainly affected by the underground mining in the western mining area.

3. By December 2011, almost the entire main shaft area had entered the movement area (the area within the movement line) after the rapid expansion stage. By December 2015, the machine room of the main shaft area entered the break area (the area within the break line), and the main

shaft had to be abandoned. When the main shaft area enters the movement area, the normal use of the main shaft and other facilities will be affected but can continue to be used after maintenance. However, when the break area expanded to encompass the main shaft area, the main shaft and other facilities could no longer be used.

4. From December 2009 to December 2011, the movement angle decreased significantly from 75.90° to 55.12° , thus becoming smaller than the designed value of 62° . From December 2010 to December 2012, the break angle changed from 87.94° to 64.62° , thus becoming smaller than the designed value of 70° . Movement and break angles are smaller than the designed values in main shaft area, resulting in cracking and abandonment of the main shaft and other facilities. The main reasons that led to the movement and break angles becoming smaller than their designed values were the larger horizontal tectonic stress and the NNW-striking joints. Therefore, in the planning and design of other metal mines, the influence of joints and tectonic stresses should be fully considered, and key buildings and facilities must be located outside the movement and break areas.

5. The rock mass in the main shaft area is cut into cantilever beams by NNW-striking joints. Toppling failure occurred in the cantilever beams due to the tectonic stress and underground mining in the western area. The cantilever beam mechanics model revealed that the rapid deformation stage of the ground in the main shaft area in December 2009 and the significant changes of the movement and break angles in 2010–2012 were due to the fracturing and toppling failure of the deep rock mass, resulting in the release of tectonic stress. Furthermore, when the exploitation reaches -600 m, the fracture width is predicted to reach 402 m.

Acknowledgements This work was supported by the National Key Research and Development Plan of China (2017YFC0805307), the National Natural Science Foundation of China (41602325, 11602284) and the Youth Innovation Promotion Association CAS (2015271).

References

- Adhikary DP, Dyskin AV (2007) Modelling of progressive and instantaneous failures of foliated rock slopes. *Rock Mech Rock Eng* 40:349–362. <https://doi.org/10.1007/s00603-006-0085-8>
- Adhikary DP, Dyskin AV, Jewell RJ, Stewart DP (1997) A study of the mechanism of flexural toppling failure of rock slopes. *Rock Mech Rock Eng* 30:75–93. <https://doi.org/10.1007/BF01020126>
- Aydan Ö, Kawamoto T (1992) The stability of slopes and underground openings against flexural toppling and their stabilisation. *Rock Mech Rock Eng* 25:143–165. <https://doi.org/10.1007/BF01019709>
- Brady BHG, Brown ET (1985) *Rock mechanics for underground mining*. George Allen Unwin, London
- Bruneau G, Tyler DB, Hadji-georgiou J, Potvin Y (2003a) Influence of faulting on a mine shaft—a case study: part I—background and instrumentation. *Int J Rock Mech Min Sci* 40:95–111. [https://doi.org/10.1016/S1365-1609\(02\)00115-6](https://doi.org/10.1016/S1365-1609(02)00115-6)

- Bruneau G, Hudyma MR, Hadjigeorgiou J, Potvin Y (2003b) Influence of faulting on a mine shaft—a case study: part II—numerical modelling. *Int J Rock Mech Min Sci* 40:113–125. [https://doi.org/10.1016/S1365-1609\(02\)00116-8](https://doi.org/10.1016/S1365-1609(02)00116-8)
- Cai M, Qiao L, Li C, Yu B, Wang S (2000) Results of in situ stress measurements and their application to mining design at five Chinese metal mines. *Int J Rock Mech Min Sci* 37:509–515. [https://doi.org/10.1016/S1365-1609\(99\)00077-5](https://doi.org/10.1016/S1365-1609(99)00077-5)
- Can E, Kuşcu Ş, Kartal ME (2012) Effects of mining subsidence on masonry buildings in Zonguldak hard coal region in Turkey. *Environ Earth Sci* 66:2503–2518. <https://doi.org/10.1007/s12665-011-1473-2>
- Chen C, Xiao G, Huang P et al (2014) Joint survey and mechanical parameters test of rock mass in west area of Chengchao iron mine. Institute of Rock and Soil Mechanics, Chinese Academy of Sciences, Wuhan
- Chen C, Xia K, Song X et al (2017) Surface subsidence monitoring and forecasting around collapse in western area of Chengchao iron mine. Institute of Rock and Soil Mechanics, Chinese Academy of Sciences, Wuhan
- Cheng G, Chen C, Ma T, Liu H, Tang C (2017) A case study on the strata movement mechanism and surface deformation regulation in Chengchao underground iron mine. *Rock Mech Rock Eng* 50:1011–1032. <https://doi.org/10.1007/s00603-016-1132-8>
- Hebblewhite BK (2001) Regional horizontal movements associated with longwall mining. University of New South Wales, Mining Research Centre, New South Wales
- Kalenchuk KS, Mckinnon S, Diederichs MS (2008) Block geometry and rock mass characterization for prediction of dilution potential into sub-level cave mine voids. *Int J Rock Mech Min Sci* 45:929–940. <https://doi.org/10.1016/j.ijrmm.2007.10.006>
- Li X, Wang SJ, Liu TY, Ma FS (2004) Engineering geology, ground surface movement and fissures induced by underground mining in the Jinchuan nickel Mine. *Eng Geol* 76:93–107. <https://doi.org/10.1016/j.enggeo.2004.06.008>
- Li WX, Zhao ST, Liang XL, Dai LF (2006) Influence of underground mining on shaft tower in Luzhong mining areas. *Chin J Rock Mech Eng* 25:74–78
- Li WX, Wen L, Liu XM, Hou XB, Liu L (2009) Regional horizontal displacements and its effect on shaft in mining areas. *Chin J Rock Mech Eng* 28(Suppl. 2):3926–3931
- Li XB, Li DY, Liu ZX (2013) Determination of the minimum thickness of crown pillar for safe exploitation of a subsea gold mine based on numerical modeling. *Int J Rock Mech Min Sci* 57:42–56
- Ma F, Deng Q, Cunningham D, Yuan R, Zhao H (2013) Vertical shaft collapse at the jinchuan nickel mine, Gansu Province, China: analysis of contributing factors and causal mechanisms. *Environ Earth Sci* 69:21–28. <https://doi.org/10.1007/s12665-012-1930-6>
- Novikov FY (1979) Pressure of thawing soils on the concrete lining of vertical mine shafts. *Eng Geol* 13:277–286. [https://doi.org/10.1016/0013-7952\(79\)90037-1](https://doi.org/10.1016/0013-7952(79)90037-1)
- Pinheiro AL, Lana MS, Sobreira FG (2015) Use of the distinct element method to study flexural toppling at the Pico Mine, Brazil. *Bull Eng Geol Environ* 74:1177–1186. <https://doi.org/10.1007/s10064-014-0713-6>
- Reid P (1998) Horizontal movements around Cataract dam, Southern Coalfield Proceedings of the MSTs 4th Triennial Conference on Buildings and Structures Subject to Ground Movement, Australia, pp 157–170
- Rejeb A, Bruel D (2001) Hydromechanical effects of shaft sinking at the Sellafeld site. *Int J Rock Mech Min Sci* 38:17–29. [https://doi.org/10.1016/S1365-1609\(00\)00061-7](https://doi.org/10.1016/S1365-1609(00)00061-7)
- Song WD, Chen CX (2013) The research report of the surface rupture mechanism and its influence on the field stability of important building in the western area of Chengchao iron mine. University of Science and Technology Beijing, Beijing
- Song XG, Chen CX, Xia KZ, Chen LL, Fu H, Deng YY, Du GM (2017) Research on deformation mechanism and feasibility to continue use mine shaft. *Rock Soil Mech* 38:331–342
- Tan WH, Kulatilake PHSW, Sun HB (2014) Influence of an inclined rock stratum on in-situ stress state in an open-pit mine. *Geotech Geol Eng* 32:31–42. <https://doi.org/10.1007/s10706-013-9689-4>
- Villegas T, Nordlund E, Dahnér-Lindqvist C (2011) Hanging wall surface subsidence at the Kiirunavaara Mine. *Sweden Eng Geol* 121:18–27. <https://doi.org/10.1016/j.enggeo.2011.04.010>
- Villegas Barba FT, Nordlund E (2013) Numerical analyses of the hanging wall failure due to sublevel caving: study case. *Int J Min Miner Eng* 4:201–223. <https://doi.org/10.1504/IJMME.2013.053168>
- Wu X, Jiang XW, Chen YF, Tian H, Xu N (2009) The influences of mining subsidence on the ecological environment and public infrastructure: a case study at the Haolaigou iron Ore Mine in Baotou, China. *Environ Earth Sci* 59:803–810. <https://doi.org/10.1007/s12665-009-0076-7>
- Xia KZ, Chen CX, Fu H, Pan Y, Deng Y (2016) Mining-induced ground deformation in tectonic stress metal mines: a case study. *Eng Geol* 210:212–230. <https://doi.org/10.1016/j.enggeo.2016.06.018>
- Xia KZ, Chen CX, Liu XM, Zheng Y, Fu H (2017) Ground movement mechanism in tectonic stress metal mines with steep structure planes. *J Cent South Univ* 24:2092–2104. <https://doi.org/10.1007/s11771-017-3618-2>
- Yao ZS, Yang JJ, Sun WL (2003) Experimental study on sliding shaft lining mechanical mechanisms underground subsidence conditions. *J Coal Sci Eng* 9:95–99
- Zhao HJ, Ma F, Xu JM (2012a) Shaft deformation and failure due to rock mass movement induced by underground backfill mining of a metal mine. *Chin J Geotech Eng* 34:340–348
- Zhao HJ, Ma FS, Xu JM, Guo J (2012b) In situ stress field inversion and its application in mining-induced rock mass movement. *Int J Rock Mech Min Sci* 53:120–128. <https://doi.org/10.1016/j.ijrmm.2012.05.005>
- Zhao HJ, Ma FS, Zhang YM, Guo J (2013) Monitoring and mechanisms of ground deformation and ground fissures induced by cut-and-fill mining in the Jinchuan Mine 2, China. *Environ Earth Sci* 68:1903–1911